

Biosafety evaluation of Janus $\text{Fe}_3\text{O}_4\text{-TiO}_2$ nanoparticles in Sprague Dawley rats after intravenous injection

Hong Su¹
 Xin Song¹
 Juan Li²
 Muhammad Zubair Iqbal²
 Samuel Selorm Fiasi
 Kenston¹
 Zhen Li¹
 Aiguo Wu²
 Min Ding³
 Jinshun Zhao¹

¹Department of Preventative Medicine, Zhejiang Key Laboratory of Pathophysiology, Medicine School of Ningbo University, Ningbo, Zhejiang, 315211, People's Republic of China; ²Key Laboratory of Magnetic Materials and Devices, Key Laboratory of Additive Manufacturing Materials of Zhejiang Province, Division of Functional Materials and Nanodevices, Ningbo Institute of Materials Technology and Engineering, Chinese Academy of Sciences, Ningbo, Zhejiang, 315201, People's Republic of China; ³Toxicology and Molecular Biology Branch, Health Effects Laboratory Division, National Institute for Occupational Safety and Health, Morgantown, WV, 26505, USA

Introduction: Newly synthesized Janus-structured $\text{Fe}_3\text{O}_4\text{-TiO}_2$ nanoparticles (NPs) appear to be a promising candidate for the diagnosis and therapy of cancer. Although the toxicity of individual Fe_3O_4 or TiO_2 NPs has been studied extensively, the toxicity of Janus $\text{Fe}_3\text{O}_4\text{-TiO}_2$ NPs is not clear.

Methods: In this study, the biosafety of both Janus $\text{Fe}_3\text{O}_4\text{-TiO}_2$ NPs (20–25 nm) and the maternal material TiO_2 NPs (7–10 nm) were evaluated in Sprague Dawley rats after one intravenous injection into the tail vein. Healthy rats were randomly divided into one control group and six experimental groups. Thirty days after treatment, rats were killed, then blood and tissue samples were collected for hematological, biochemical, element-content, histopathological, and Western blot analysis.

Results: The results show that only a slight Ti element accumulation in the heart, spleen, and liver could be found in the Janus $\text{Fe}_3\text{O}_4\text{-TiO}_2$ NP groups ($P>0.05$ compared with control). However, significant Ti element accumulation in the spleen, lungs, and liver was found in the TiO_2 NP-treated rats. Both $\text{Fe}_3\text{O}_4\text{-TiO}_2$ NPs and TiO_2 NPs could induce certain histopathological abnormalities. Western blot analysis showed that both NPs could induce certain apoptotic or inflammatory-related molecular protein upregulation in rat livers. A certain degree of alterations in liver function and electrolyte and lipid parameters was also observed in rats treated with both materials. However, compared to Janus structure $\text{Fe}_3\text{O}_4\text{-TiO}_2$ NP-treated groups, TiO_2 NPs at 30 mg/kg showed more severe adverse effects.

Conclusion: Our results showed that under a low dose (5 mg/kg), both NP types had no significant toxicity in rats. Janus NPs certainly seem less toxic than TiO_2 NPs in rats at 30 mg/kg. To ensure safe use of these newly developed Janus NPs in cancer diagnosis and therapy, further animal studies are needed to evaluate long-term bioeffects.

Keywords: $\text{Fe}_3\text{O}_4\text{-TiO}_2$ NPs, Janus structure NPs, TiO_2 NPs, accumulation, inductively coupled plasma mass spectrometry, ICP-MS, biodistribution, nanomedicine

Introduction

Nanotechnology has been labeled the new technology of the 21st century. With the rapid development of nanotechnology, potential applications of nanomaterials in medicine have been researched widely in recent years.¹ Nanomaterials have developed rapidly, and traditional nanomaterials are now unable to meet the needs of some special industries or high technology. Multifunctional Janus nanoparticles (NPs) have become a hot spot in the research field of nanomaterials in recent years.^{2,3} Due to their fascinating hierarchical superstructures, Janus particles are promising candidates for a variety of high-quality applications, such as catalysis, textiles, sensors, therapeutic treatments,

Correspondence: Jinshun Zhao
 Department of Preventative Medicine, Zhejiang Key Laboratory of Pathophysiology, Medicine School of Ningbo University, 818 Fenghua Road, Ningbo, Zhejiang, 315211, People's Republic of China
 Tel +86 574 8760 9591
 Fax +86 574 8760 8638
 Email zhaojinshun@nbu.edu.cn

and imaging diagnosis.^{4,5} Recently, Janus NPs have gained extensive attention in the field of chemistry and biology, resulting from combined chemical, magnetic, optical, and electronic interactions at the solid-state heterojunction of the particles.⁶ In this system, two or more nanocomponents with different properties are linked together, which allows the simultaneous realization of multiple functions. In particular, Janus nanostructures may introduce dual- or multimodal responses to enable diagnostics and therapeutics to be performed simultaneously for biomedical applications.⁷

Because of their excellent optical performance and electrical properties, TiO_2 NPs have a wide range of applications. Nanosized particles have been used for the photodynamic and sonodynamic treatment of preclinical cancer.^{8,9} Photodynamic therapy (PDT) is a method of joint use of light and special drugs (photosensitizers) for the treatment of diseased cells and tissue therapy.¹⁰ The application of TiO_2 NPs in the field of antitumor therapy has aroused widespread concern. The field of molecular imaging has been gaining interest in the research world. Magnetic resonance imaging (MRI)-contrast agents can increase diagnostic accuracy and imaging sensitivity for detecting pathological changes and also provide previously undetectable physiological information.¹¹ Superparamagnetic iron oxide has been classified as biocompatible, because it is processed by cells as part of physiological iron metabolism, has good chemical stability and better magnetic responsiveness, and requires only nanomolar concentrations to produce good images.^{12,13}

In our previous work, multifunctional $\text{Fe}_3\text{O}_4\text{-TiO}_2$ NPs with Janus structure for MRI and potential PDT were synthesized, using Fe_3O_4 as the MRI-contrast agent and TiO_2 as an inorganic photosensitizer for PDT.¹⁴ The results showed that $\text{Fe}_3\text{O}_4\text{-TiO}_2$ NPs had good T_2 -weighted MRI performance and MCF7 cells incubated with $\text{Fe}_3\text{O}_4\text{-TiO}_2$ NPs were killed under ultraviolet-light irradiation. Compared with traditional organic photosensitizers, inorganic TiO_2 photosensitizers have more stable PDT performance due to their nanosize and antiphotodegradable stability.¹⁵ However, *in vivo* biomedical applications using TiO_2 NPs have been limited because of shallow penetration and ultraviolet light being a well-known mutagen.

Due to the promising multifunctional properties of Janus $\text{Fe}_3\text{O}_4\text{-TiO}_2$ NPs in cancer diagnosis and treatment, *in vitro* and *in vivo* toxicity and biodistribution of this material should be thoroughly evaluated before providing basic information for its bioapplication in the future. As we know, few NPs should be applied biologically in humans due to their widely known toxicity. Interestingly, while the toxicity of single TiO_2 NPs or Fe_3O_4 NPs has been widely

studied, toxicity evaluation on Janus $\text{Fe}_3\text{O}_4\text{-TiO}_2$ NPs is still lacking.^{16–19} Janus $\text{Fe}_3\text{O}_4\text{-TiO}_2$ NPs will be used mainly through intravenous injection for diagnosis and treatment in medicine. Intravenous injection of nanomaterials directly into the blood without passing through the normal absorption process has raised public concerns regarding the toxicity to humans in nanomedicine.²⁰ In this study, rats were treated with intravenous tail injections with a single dose of Janus $\text{Fe}_3\text{O}_4\text{-TiO}_2$ NPs or TiO_2 NPs in saline. Thirty days after treatment, rats were killed, then hematological, biochemical, element-content, histopathological, and molecular protein expression were analyzed.

Methods

Materials

Biochemical and hematological analyses were performed with a 7600-110 autoanalyzer (Hitachi Ltd., Tokyo, Japan) and blood analyzer (XT-1800i; Sysmex Corporation, Kobe, Japan), respectively. Metal content (Ti and Fe) was detected by inductively coupled plasma (ICP) mass spectrometry (MS; Nexion 300D; PerkinElmer Inc., Waltham, MA, USA) and ICP optical emission spectroscopy (Optima 2100DV; PerkinElmer Inc.). The monoclonal antibodies p38, phosphorylated p38 (p-p38), JNK, phosphorylated JNK (p-JNK), ERK, HO1, c-Jun, cleaved caspase 3, Bcl2, Bax, p50, p53, Nrf2, Akt, and GAPDH were obtained from Cell Signaling Technology (Danvers, MA, USA). Sprague Dawley rats were obtained from Zhejiang Provincial Laboratory Animal Science Center (Hangzhou, China). $\text{Fe}_3\text{O}_4\text{-TiO}_2$ NPs and TiO_2 NPs were obtained from our cooperation team at the Chinese Academy of Materials (Ningbo, China).

$\text{Fe}_3\text{O}_4\text{-TiO}_2$ NP and TiO_2 NP preparation

$\text{Fe}_3\text{O}_4\text{-TiO}_2$ composite NPs were synthesized by the solvent-thermal method as stated in our previous work.¹⁴ First, TiO_2 NPs (about 7–10 nm) were synthesized based on a previously reported method.²¹ Then, prepared TiO_2 NPs were centrifuged and washed with ethanol and redispersed in 10 mL *n*-hexane. Next, ferric acetylacetone (17 mg) was dissolved in oleic acid (4 mL) and *n*-octyl alcohol (12 mL), then added to a Teflon tube that had been autoclaved for 3 hours at 240°C. Then, the mixture was washed with ethanol and dispersed into a nonpolar solvent. TiO_2 NPs (1 mL dispersed in *n*-hexane) were dropped into the ferric acetylacetone solution. The mixture was stirred for 4 hours before increasing the temperature to 70°C, in order to evaporate the *n*-hexane. Finally, the mixture was cooled to room temperature and transferred into a reaction kettle. The reaction temperature was kept at 240°C for 3 hours. Finally, the prepared $\text{Fe}_3\text{O}_4\text{-TiO}_2$ NPs were centrifuged,

washed with ethanol three times, and dispersed into 10 mL cyclohexane. Later, F127 triblock polymer was used to transfer the phase from organic to aqueous. $\text{Fe}_3\text{O}_4\text{-TiO}_2$ NPs (1 mL) were added dropwise to F127 (700 mg) and dispersed in CHCl_3 (70 mL). After the solution had been stirred for 4 hours, water (10 mL) was added and CHCl_3 evaporated using a rotatory evaporator. Finally, the aqueous dispersed NPs were washed with ethanol and redispersed in water.

Detection of size distribution

High-resolution transmission electron microscopy (HRTEM) of NPs was obtained with a 2100 microscope (JEOL, Tokyo, Japan) at 200 kV. X-ray diffraction patterns were collected on a D8 Advance (Bruker, Billerica, MA, USA) powder diffractometer using $\text{CuK}\alpha$ radiation (40 kV, 40 mA) with a step size of 0.02° in 2θ and 3 seconds/step. Loaded Fe and Ti content in $\text{Fe}_3\text{O}_4\text{-TiO}_2$ NPs was measured by ICP optical emission spectroscopy.

Experimental design and preparation

All animals were kept in stress-free, hygienic, and animal-friendly conditions (relative humidity $60\%\pm10\%$, room temperature $20^\circ\text{C}\pm2^\circ\text{C}$, and 12-hour light/dark cycle). Food and water were available ad libitum. All animal-study protocols were approved by the Ningbo University Institutional Animal Care and Use Committee (AEWC-2016-151), and experiments followed the Chinese “Regulation on the management of laboratory animals”, adopted in 1988. Healthy male rats (12 weeks old) were selected and randomly divided into one control group and six experimental groups (5, 15, and 30 mg/kg $\text{Fe}_3\text{O}_4\text{-TiO}_2$ NPs or TiO_2 NPs, respectively) with six rats in each group. The observation period was 30 days. A staged approach to dosing method was used for selection of the dose ranges. When determining chemical dosage, care was taken to prevent any severe toxicity in the animal that could affect absorption, metabolism, distribution, or excretion.²² Following this principle, the highest treatment dose for both NP types was set at 30 mg/kg for this study. $\text{Fe}_3\text{O}_4\text{-TiO}_2$ NPs and TiO_2 NPs were suspended in normal saline and vortexed. Nanomaterials were administered intravenously into the tail vein. The control group received the same amount of saline (2 mL/rat) as treated groups.

Organ weight:body weight coefficients and hematological, biochemical, and electrolyte analysis

At the end of the experiment, the body weights of all rats were recorded before the rats were killed. The average weight of rats from the control group was 417.16 ± 11.53 g, and the

average weights of the three TiO_2 NP groups and three $\text{Fe}_3\text{O}_4\text{-TiO}_2$ NP groups were 399.16 ± 13.56 g, 401.50 ± 16.48 g, 409.80 ± 26.60 g, 427.83 ± 23.16 g, 396.71 ± 27.86 g, and 413.80 ± 25.74 g, respectively. No significant difference in body weight was found among the seven animal groups. Rats were anesthetized with chloral hydrate by intraperitoneal injection. Blood was collected for hematological, biochemical, and electrolyte analysis in anticoagulant or coagulation-promoting test tubes. Blood was analyzed for hematological parameters using the Sysmex XT-1800i. Enzymatic parameters related to liver, kidney, and cardiac function were detected using the Hitachi 7600-110, and lipid- and serum-electrolyte analysis was also included. Then, rats were killed, and brains, hearts, livers, spleens, lungs, kidneys, and testes taken out and weighed immediately. Organ weight:body weight coefficients were calculated as the ratio of wet-tissue weight (g) to body weight (100 g).

ICP-MS

Tissue samples (0.5 g) of brain, heart, liver, spleen, lungs, kidneys, and testes were weighed and digested with 5 mL HNO_3 in a test tube overnight. The mixture was stirred and heated at reflux at 170°C for 1 hour and then diluted to 50 mL with deionized water. Tissue-sample tubes were washed three times in deionized water.

Histopathological examination

After weighing, organs were fixed immediately in 10% formalin for histopathological examination. Tissue samples were examined to check pathological effects caused by different treatments. Formalin-fixed tissue was stored at 4°C until examination. Tissue samples were processed using standard histological laboratory techniques. Using a microtome, tissue sections were cut to approximately 3–4 μm thickness, then stained with H&E using a standard protocol.

Western blot analysis

Liver-tissue samples were frozen in liquid nitrogen and stored at -80°C until use. Tissue samples (20–30 mg) were ground with a mortar and pestle in liquid nitrogen. Lysis buffer (100 μL) containing phenylmethylsulfonyl fluoride (10 mmol/L) and EDTA (1 mM) was then added to the tissue residue for 4 hours. Then, the lysate was centrifuged at 12,000 rpm for 15 minutes at 4°C to obtain the supernatant. Protein concentrations of the supernatant were determined by the bicinchoninic acid method. The supernatant was mixed with 5× loading buffer (4:1 in volume) and boiled for 5 minutes for Western blot. Polyacrylamide-stacking (6%) gels and resolving (10%) gels were used to separate the proteins of different

molecular weights. Immunoblots for expression of p38, p-p38, JNK, p-JNK, HO-1, ERK, c-Jun, cleaved caspase 3, Bcl2, Bax, P50, p53, Nrf2, Akt, and GAPDH were detected. All antibodies for Western blot in this study were purchased from Cell Signaling Technology. Tris-buffered saline Tween 20 with 5% skim milk was used to block the membranes for 3.5 hours before incubation overnight with primary antibodies (1:1,000 dilution). After three washes with Tris-buffered saline Tween 20, membranes were incubated with the corresponding secondary antibodies (1:4,000 dilution) for 1.5 hours. A 4200SF imaging processing system (Tanon, Shanghai, China) was used for Western blot analysis.

Statistical analysis

Statistical analysis was performed using SPSS 16.0. One-way ANOVAs were used for organ-coefficient comparison and hematological, biochemical, electrolyte, and accumulation analysis. Student's *t*-test was used to compare differences between experimental groups and the control group. $P<0.05$ was considered statistically significant. Results are presented as means \pm SD.

Results

Average size distribution of Fe_3O_4 - TiO_2 NPs

Images of Fe_3O_4 - TiO_2 NPs were captured by TEM and HRTEM (Figure 1). Figure 1A shows that most of the Fe_3O_4 - TiO_2 NPs had a Janus structure and Fe_3O_4 had cubic spherical particles and narrower particle-size distribution. The average size distribution of the Fe_3O_4 - TiO_2 NPs was about 20–25 nm, detected using a Tecnai F20 with energy-dispersive spectroscopy. As such, the experimental materials met the requirements to be classified as NPs. Figure 1B shows the HRTEM of Fe_3O_4 - TiO_2 NPs and shows that Fe_3O_4 was coupled with TiO_2 NPs to form a Janus structure.

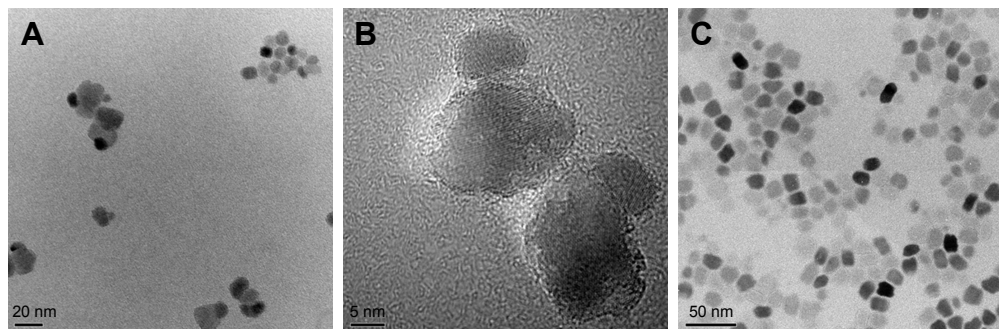


Figure 1 Images of Fe_3O_4 - TiO_2 NPs and TiO_2 NPs captured by TEM and HRTEM.

Notes: (A) TEM of Fe_3O_4 - TiO_2 NPs; (B) HRTEM of Fe_3O_4 - TiO_2 NPs; (C) TEM of TiO_2 NPs.

Abbreviations: HRTEM, high-resolution TEM; NPs, nanoparticles; TEM, transmission electron microscopy.

Figure 1C shows that average TiO_2 NP size distribution was about 7–10 nm, the particles well dispersed, and no reunion of TiO_2 NPs was observed. Figure 2 shows the X-ray diffraction spectra of Fe_3O_4 - TiO_2 NPs, Fe_3O_4 NPs, and TiO_2 NPs. It can be observed that the peaks of Fe_3O_4 - TiO_2 NPs include TiO_2 peaks with anatase structure and Fe_3O_4 peaks with cubic structure.

Organ weight:body weight coefficients

Organ weight:body weight coefficients of the rats are shown in Table 1. No significant differences were found in organ coefficients of the heart, lungs, kidneys, brain, or testes in Fe_3O_4 - TiO_2 NPs or TiO_2 NPs compared to the control group. In 15 mg/kg Fe_3O_4 - TiO_2 NPs, liver and spleen coefficients were higher than the control group ($P<0.05$).

Hematological analysis

Hematological effects are shown in Table 2. Only in 5 mg/kg TiO_2 NPs was the white blood cell (WBC) count significantly less than that of the control group. There was no significant change in any other hematological parameter.

Biochemical analysis

Biochemical parameters of liver, renal, lipid, cardiac, and electrolyte profiles are shown in Table 3. Liver profiles showed that no significant difference in serum levels of total bilirubin, albumin, or total protein was observed in any of the treated animals. In the TiO_2 NP-treated groups, Alanine aminotransferase (ALT) at 5 and 30 mg/kg and AST at 30 mg/kg were significantly elevated. In the Fe_3O_4 - TiO_2 NP-treated groups, aspartate transaminase (AST) at 5 and 30 mg/kg and ALT in all treated groups were significantly decreased. Alkaline phosphatase (ALP) showed no significant difference among any of the treatment groups. Renal profiles showed that uric acid (UrcA) in the Fe_3O_4 - TiO_2 NP-treated groups

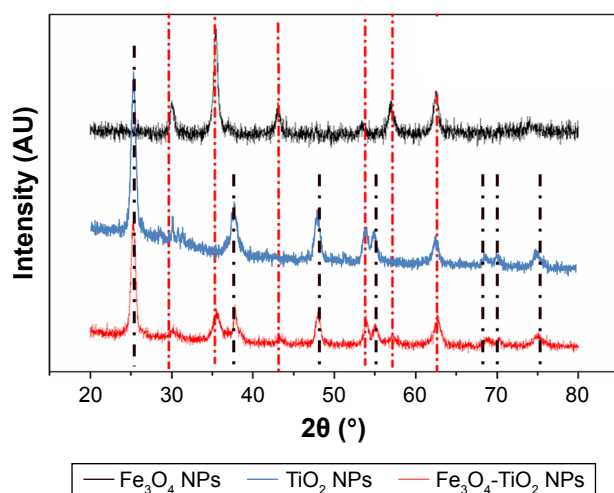


Figure 2 $\text{Fe}_3\text{O}_4\text{-TiO}_2$ NPs captured by X-ray diffraction.

Abbreviation: NPs, nanoparticles.

was significantly decreased. Serum low-density-lipoprotein cholesterol (LDL-C) levels in TiO_2 NP-treated rats at 5 mg/kg and $\text{Fe}_3\text{O}_4\text{-TiO}_2$ NPs at 30 mg/kg were significantly higher than the control group. No significant changes were observed for triglycerides or high-density-lipoprotein cholesterol levels in any of the animals treated.

All treated animals showed a slight decrease in serum creatine kinase (CK) levels, but only TiO_2 NPs at 5 mg/kg showed a significant decrease when compared to control. $\text{Fe}_3\text{O}_4\text{-TiO}_2$ NPs in all treatment groups significantly decreased serum CK-MB levels, while TiO_2 NPs only at 30 mg/kg serum CK-MB levels decreased when compared with the control group. Serum-potassium levels in $\text{Fe}_3\text{O}_4\text{-TiO}_2$ NPs at 15 mg/kg were significantly lower than in the control group. Serum-magnesium levels in all treated animals showed a decrease, but no statistical significance was found. Serum-phosphorus levels in $\text{Fe}_3\text{O}_4\text{-TiO}_2$ NP-treated rats at 5 and 30 mg/kg were significantly decreased when compared to the control group.

Table 1 Organ weight:body weight coefficients of rats after 30 days' exposure to $\text{Fe}_3\text{O}_4\text{-TiO}_2$ NPs or TiO_2 NPs through intravenous injection

Parameters	Control (mg/kg)	TiO_2 NPs (mg/kg)			$\text{Fe}_3\text{O}_4\text{-TiO}_2$ NPs (mg/kg)		
		5	15	30	5	15	30
Heart	3.28±0.35	3.29±0.21	3.37±0.33	3.45±0.30	3.32±0.16	3.58±0.38	3.23±0.25
Liver	31.80±1.45	33.30±1.48	32.10±2.98	34.40±2.46	34.70±1.73	35.50±1.55*	33.60±1.67
Spleen	1.95±0.25	2.31±0.42	2.13±0.37	2.17±0.11	2.20±0.57	2.79±0.88*	2.12±0.16
Lung	3.79±0.40	3.42±0.42	3.69±0.48	3.37±0.16	3.35±0.47	3.80±0.62	3.20±0.28
Kidney	6.45±0.28	6.81±0.67	6.86±0.74	6.63±0.35	6.38±0.41	6.69±0.31	6.13±0.51
Brain	4.23±0.61	4.23±0.66	4.60±0.80	4.78±0.43	4.46±0.50	4.94±0.33	4.59±0.15
Testis	6.13±1.02	7.12±0.48	6.85±0.58	6.99±0.50	6.49±0.40	6.91±0.79	6.85±0.36

Note: Results given as means ± SD (* $P<0.05$ compared with control).

Abbreviation: NPs, nanoparticles.

Analysis of metal content in tissue

Total Ti levels in tissue were used for evaluating the presence or distribution of Ti composed in $\text{Fe}_3\text{O}_4\text{-TiO}_2$ NPs and TiO_2 NPs in the body. Ti content in different tissue types is shown in Figure 3. After treatment with $\text{Fe}_3\text{O}_4\text{-TiO}_2$ NPs or TiO_2 NPs, Ti levels in cardiac tissue showed a tendency to increase in all treated animals in a dose-related manner, although no statistical significance was found, which might have been due to individual differences. Ti content in the liver in TiO_2 NP-treated animals at 15 and 30 mg/kg showed a significant elevation ($P<0.05$). Although Ti content also showed a tendency to increase in the livers of $\text{Fe}_3\text{O}_4\text{-TiO}_2$ NP-treated animals, no statistical significance was found. In spleens and lungs of the TiO_2 NP-treated animals, Ti content was significantly increased at 15 and 30 mg/kg. No significant difference was found in Ti content in spleens and lungs in any $\text{Fe}_3\text{O}_4\text{-TiO}_2$ NP-treated groups. Treatments of $\text{Fe}_3\text{O}_4\text{-TiO}_2$ NPs or TiO_2 NPs resulted in only a slight change in Ti content in the brain and testes ($P>0.05$).

In addition, Figure 3 also indicates that at 30 days after treatment, TiO_2 NPs had still not excreted entirely from the body. Accumulative ability of Ti in different organs ranked as liver > spleen > lungs > heart > kidneys > brain > testes. Fe content in rat tissue is shown in Figure 4. After treatment, no significant change in Fe content in the heart, liver, spleen, lungs, kidneys, brain, or testes was found in any of the TiO_2 NP- or $\text{Fe}_3\text{O}_4\text{-TiO}_2$ NP-treatment groups, except for TiO_2 NP-treated rats at 30 mg/kg, which showed a significant decrease. Fe content in different organs ranked as spleen > heart > lungs > kidneys > brain > testes > liver.

Histopathological examination

Liver histopathological images are shown in Figure 5. At 5 mg/kg, liver tissue in $\text{Fe}_3\text{O}_4\text{-TiO}_2$ NP-treated rats had no obvious abnormal pathological changes compared with the

Table 2 Hematological analysis after different treatments

Parameters	Control	TiO ₂ NPs (mg/kg)			Fe ₃ O ₄ -TiO ₂ NPs (mg/kg)		
		5	15	30	5	15	30
WBCs ($\times 10^9/L$)	10.72 \pm 2.56	7.38 \pm 1.35 ^a	8.76 \pm 1.72	8.24 \pm 1.76	8.78 \pm 1.29	8.79 \pm 2.21	11.66 \pm 2.28
Neutrophils (%)	14.86 \pm 7.15	17.07 \pm 7.20	19.42 \pm 9.34	20.10 \pm 7.47	23.23 \pm 4.82	16.96 \pm 5.83	22.36 \pm 6.58
Lymphocytes (%)	83.56 \pm 2.83	79.53 \pm 8.50	84.40 \pm 3.78	81.36 \pm 6.27	76.45 \pm 5.19	80.17 \pm 3.05	77.84 \pm 5.82
Monocytes (%)	2.22 \pm 1.60	1.97 \pm 0.97	3.38 \pm 1.58	2.88 \pm 0.64	1.68 \pm 2.20	3.31 \pm 1.73	2.90 \pm 2.68
Eosinophils (%)	0.88 \pm 0.26	0.53 \pm 0.26	0.94 \pm 0.29	2.25 \pm 3.87	0.87 \pm 0.51	0.79 \pm 0.32	0.92 \pm 0.37
Basophils (%)	0.10 \pm 0.07	0.12 \pm 0.15	0.04 \pm 0.05	0.08 \pm 0.04	0.05 \pm 0.05	0.09 \pm 0.04	0.06 \pm 0.05
Neutrophils (%)	1.53 \pm 0.90	1.26 \pm 0.56	1.68 \pm 0.74	1.59 \pm 0.47	2.08 \pm 0.61	1.43 \pm 0.46	2.66 \pm 1.01
Lymphocytes (%)	8.36 \pm 0.79	5.79 \pm 1.42 ^a	7.30 \pm 1.41	6.61 \pm 1.51	6.49 \pm 0.74	7.02 \pm 1.94	8.84 \pm 1.52
Monocytes (%)	0.22 \pm 0.16	0.16 \pm 0.11	0.29 \pm 0.13	0.24 \pm 0.10	0.14 \pm 0.19	0.32 \pm 0.20	0.35 \pm 0.37
Eosinophils (%)	0.09 \pm 0.03	0.03 \pm 0.02	0.08 \pm 0.03	0.21 \pm 0.36	0.08 \pm 0.05	0.07 \pm 0.04	0.10 \pm 0.03
RBCs ($\times 10^{12}/L$)	7.51 \pm 0.14	7.18 \pm 0.57	7.46 \pm 0.44	7.45 \pm 0.24	7.26 \pm 0.90	7.11 \pm 0.67	7.01 \pm 0.68
Hb (g/L)	141.80 \pm 5.12	138.83 \pm 10.07	138.04 \pm 5.60	140.80 \pm 7.40	138.17 \pm 14.12	132.57 \pm 11.00	133.20 \pm 15.47
Hematocrit	0.44 \pm 0.01	0.43 \pm 0.03	0.43 \pm 0.02	0.44 \pm 0.02	0.43 \pm 0.03	0.42 \pm 0.03	0.42 \pm 0.04
MCV (fL)	58.64 \pm 1.68	59.70 \pm 1.73	57.92 \pm 2.00	58.50 \pm 1.20	59.78 \pm 3.76	58.39 \pm 2.62	60.22 \pm 1.68
MCH (pg)	18.86 \pm 0.71	19.38 \pm 0.56	18.56 \pm 0.73	18.92 \pm 0.63	19.12 \pm 0.62	18.66 \pm 0.60	18.94 \pm 0.59
MCHC (g/L)	321.60 \pm 4.88	324.83 \pm 3.97	320.80 \pm 4.44	323.00 \pm 4.30	319.83 \pm 9.95	319.57 \pm 5.71	314.80 \pm 11.43
RDW-CV (%)	13.26 \pm 0.63	13.37 \pm 0.45	13.34 \pm 0.44	13.16 \pm 0.34	14.32 \pm 3.38	14.00 \pm 1.04	14.98 \pm 2.93
Platelet count ($\times 10^9/L$)	751.20 \pm 239.82	630.67 \pm 159.65	736.00 \pm 104.9	545.60 \pm 261.68	586.00 \pm 189.9	727.57 \pm 84.60	756.60 \pm 74.29
PDW-CV (%)	14.94 \pm 0.05	14.90 \pm 0.09	14.88 \pm 0.08	14.96 \pm 0.13	14.95 \pm 0.08	14.81 \pm 0.11	14.88 \pm 0.18
MPV (fL)	6.88 \pm 0.08	6.83 \pm 0.08	6.86 \pm 0.18	6.86 \pm 0.25	6.78 \pm 0.12	6.73 \pm 0.11	6.76 \pm 0.25
Plateletcrit (%)	0.57 \pm 0.18	0.48 \pm 0.13	0.56 \pm 0.17	0.42 \pm 0.20	0.44 \pm 0.14	0.54 \pm 0.06	0.57 \pm 0.06

Notes: Results given as means \pm SD (* P <0.05 compared with control).

Abbreviations: Hb, hemoglobin; MCH, mean corpuscular Hb; MCHC, MCH concentration; MCV, mean corpuscular volume; MPV, mean platelet volume; NPs, nanoparticles; PDW-CV, platelet-distribution width coefficient of variation; RBCs, red BCs; RDW-CV, RBC-distribution-width coefficient of variation; WBCs, white blood cells.

control. However, at the high treatment dose (30 mg/kg), Fe₃O₄-TiO₂ NPs induced certain lymphocytic infiltration at the periphery of the liver. Small focal-like inflammatory cell infiltration appeared around the portal area or hepatic vein in the 5 and 15 mg/kg TiO₂ NP groups. Lymphocyte aggregation was observed in the 30 mg/kg TiO₂ NP group. TiO₂ NPs induced more severe adverse changes than Fe₃O₄-TiO₂ NPs at the same treatment dose.

Lung histopathological images are illustrated in Figure 6. TiO₂ NPs at 15 and 30 mg/kg induced inflammatory cell infiltration around blood vessels of lung tissue, cell-nodule formation, smaller alveoli, and thicker interstitium when compared with the control group. At 30 mg/kg, Fe₃O₄-TiO₂ NPs showed similar effects of alveoli getting smaller and interstitium getting thicker.

Spleen histopathological images are shown in Figure 7. Increased red-pulp area and severe congestion were observed in both TiO₂ NP- and Fe₃O₄-TiO₂ NP-treated animals at 15 and 30 mg/kg. Comparatively, at the same treatment dose, TiO₂ NPs induced more severe adverse changes than Fe₃O₄-TiO₂ NPs.

Histopathological results for the kidneys are shown in Figure 8. As the dose of TiO₂ NPs increased, the volume of

glomerular and number of cells increased. At 30 mg/kg in both Fe₃O₄-TiO₂ NP and TiO₂ NP groups, renal tubular epithelial cells were cloudy and swollen. In TiO₂ NP-treated animals, granule denaturation and membrane vacuolar degeneration were observed in the epithelial cells of the renal tubule.

Western blot analysis

Western blot analysis on protein expression of p38, p-p38, JNK, p-JNK, HO-1, ERK, c-Jun, cleaved caspase 3, Bcl2, Bax, p50, p53, Nrf2, Akt, and GAPDH in liver tissue is shown in Figure 9. Significant increases in the expression of p-p38, JNK, p-JNK, HO1, c-Jun, cleaved caspase 3, Bax, p50, and p53 was observed in both Fe₃O₄-TiO₂ NP- and TiO₂ NP-treated groups with a dose relationship when compared to the control group. An increase in ERK expression was observed only in 5 mg/kg TiO₂ NP- and 15 and 30 mg/kg Fe₃O₄-TiO₂ NP-treated animals. Both Fe₃O₄-TiO₂ NPs and TiO₂ NPs significantly decreased Bcl2 in a dose-related manner. No obvious effects of p38 or Nrf2 expression were observed in Fe₃O₄-TiO₂ NP- or TiO₂ NP-treated animals. Similarly to ERK expression, Akt expression was enhanced in 5 mg/kg TiO₂ NP- and 15 and 30 mg/kg Fe₃O₄-TiO₂ NP-treated animals.

Table 3 Biochemical analysis of liver, renal, and lipid profiles

Parameters	Control	TiO_2 NPs (mg/kg)			$\text{Fe}_3\text{O}_4\text{-TiO}_2$ NPs (mg/kg)		
		5	15	30	5	15	30
Liver profile							
TBil (μmol/L)	1.37±0.46	1.28±0.63	0.90±0.37	1.82±0.91	1.18±0.61	1.96±0.74	1.64±1.03
TP (g/L)	51.68±1.50	51.47±0.68	51.23±2.2	52.20±1.35	51.32±2.80	50.41±1.8	49.40±1.40
Alb (g/L)	26.85±1.04	27.03±0.19	26.25±1.43	27.52±0.79	26.68±1.34	25.41±1.22	25.7±1.22
Glob (g/L)	24.83±0.74	24.43±0.58	24.98±1.04	24.68±1.04	24.63±1.58	25.00±2.69	23.70±0.60
ALT (U/L)	50.83±5.78	47.00±5.40	46.33±5.05	36.40±2.19 ^b	42.00±4.52 ^a	44.86±5.08	37.6±6.11 ^b
AST (U/L)	134.00±29.40	99.00±15.92 ^b	110.17±9.58	83.00±11.38 ^b	94.00±11.28 ^b	95.00±14.10 ^b	91.20±6.34 ^b
AST/ALT	2.62±0.42	2.11±0.23 ^a	2.40±0.28	2.29±0.37	2.24±0.09	2.12±0.27 ^a	2.47±0.37
ALP (U/L)	289.83±28.30	297.67±70.11	247.83±42.40	274.80±61.65	273.33±52.34	318.00±84.06	224.80±30.03
Renal profile							
Urea nitrogen (mmol/L)	7.15±0.36	6.49±0.74	5.71±0.45 ^b	6.03±0.61 ^b	6.62±0.31	6.18±0.57 ^a	6.31±0.57
Creatinine (μmol/L)	35.56±7.00	28.27±3.82 ^a	28.65±5.47	28.28±3.10	29.85±5.12	29.69±3.15	30.80±3.02
UrcA (μmmol/L)	166.17±64.13	115.33±12.29	124.00±19.12	119.60±13.92	105.67±32.44 ^b	99.57±14.37 ^b	98.80±22.63 ^b
Lipid profile							
Chol (mmol/L)	1.35±0.16	1.50±0.06	1.33±0.20	1.39±0.16	1.33±0.11	1.32±0.16	1.59±0.31
TG (mmol/L)	0.90±0.29	0.77±0.27	0.80±0.14	0.78±0.28	1.08±0.28	0.94±0.24	1.06±0.29
HDL-C (mmol/L)	0.47±0.05	0.49±0.03	0.44±0.08	0.47±0.07	0.45±0.03	0.48±0.08	0.51±0.13
LDL-C (mmol/L)	0.43±0.04	0.52±0.05 ^a	0.46±0.08	0.46±0.05	0.45±0.04	0.46±0.05	0.57±0.10 ^b
Glucose (mmol/L)	12.87±2.71	10.08±1.70 ^a	11.10±0.62	10.85±1.05	11.58±1.19	11.34±1.38	11.34±1.33
Cardiac profile							
CK (U/L)	3,589.80± 1,758.30	1,881.20± 897.60 ^a	3,019.30± 328.05	2,096.00± 617.80	2,588.00± 1,100.70	2,252.70± 873.01	2,145.00± 377.16
CK-MB (U/L)	645.83±149.36	499.00±82.98	526.17±72.96	410.20±66.94 ^b	410.67±96.97 ^b	397.71±99.94 ^b	419.60±92.29 ^b
Amy (U)	2,457.67± 162.98	2,422.33± 237.82	2,333.17± 255.11	2,427.60± 150.82	2,384.33± 145.86	2,353.14± 76.40	2,443.80±
GPDA (U/L)	74.33±11.84	74.67±8.24	73.33±14.56	78.20±11.08	77.83±12.70	78.00±14.21	67.40±17.39
Electrolyte profile							
K (mmol/L)	9.41±0.54	8.63±0.46	8.55±0.55	7.89±0.36	8.87±2.36	7.66±0.53 ^a	8.48±1.33
Cl (mmol/L)	98.52±0.84	100.90±0.63	99.95±1.18	100.58±1.11	100.97±1.24	100.70±3.14	101.42±2.12 ^a
Ca (mmol/L)	2.46±0.08	2.52±0.01	2.51±0.07	2.54±0.08	2.53±0.09	2.49±0.06	2.49±0.09
Mg (mmol/L)	0.90±0.08	0.83±0.04	0.87±0.05	0.86±0.05	0.87±0.05	0.86±0.07	0.84±0.05
P (mmol/L)	2.51±0.18	2.16±0.14 ^a	2.43±0.22	2.37±0.22	2.07±0.20 ^b	2.23±0.24	2.09±0.29 ^a

Notes: Results given as means ± SD (^a $P<0.05$, ^b $P<0.01$ compared with control).

Abbreviations: Alb, albumin; ALP, alkaline phosphatase; ALT, alanine aminotransferase; Amy, amylase; AST, aspartate transaminase; Chol, total cholesterol; CK, creatine kinase; CK-MB, creatinine kinase; Glob, globulin; GPDA, glycylproline dipeptidyl aminopeptidase; HDL-C, high-density-lipoprotein cholesterol; LDL-C, low-density-lipoprotein cholesterol; MB isoenzyme; TBil, total bilirubin; TG, triglycerides; TP, total protein; UrcA, uric acid.

Discussion

In view of the potential applications of Janus $\text{Fe}_3\text{O}_4\text{-TiO}_2$ NPs in the diagnosis and treatment of cancer, biosafety evaluation on these newly developed Janus NPs through intravenous injection in rats was conducted. Research has shown that intravenous injection of $\text{Fe}_3\text{O}_4\text{-TiO}_2$ NPs is a practical method for radiotherapy.²³ In order to compare maternal with synthesized material, TiO_2 NPs used to synthesize $\text{Fe}_3\text{O}_4\text{-TiO}_2$ NPs were also evaluated in this study.

Intravenous injection of $\text{Fe}_3\text{O}_4\text{-TiO}_2$ NPs induced liver injury

At 30 days after treatment, all rats had survived. In the first 2 days after 30 mg/kg intravenous injection, toxic symptoms indicated by less physical activity and less intake of food and water were observed in some of the $\text{Fe}_3\text{O}_4\text{-TiO}_2$ NP- and TiO_2

NP-treated animals compared to the control group. In this study, we found that in the 15 mg/kg $\text{Fe}_3\text{O}_4\text{-TiO}_2$ NP group, liver coefficients of rats were significantly higher than the control group. This was consistent with histopathological results of distortion of normal liver architecture due to congestion and a decrease in liver sinusoids compared to the controls. In hematological analysis, a significant decrease in WBCs and lymphocytes was found in the 5 mg/kg TiO_2 NP-treatment group. Other TiO_2 NP-treated animals also showed a slight decrease in these two parameters, but with no significant difference. Studies suggest that a low WBC count is usually the result of a medical condition that disrupts the function of the bone marrow or destroys WBCs. These conditions may include infections, congenital disorders, certain cancers, cancer therapies, and certain drug administration.^{24,25} A low lymphocyte or WBC count may increase the body's

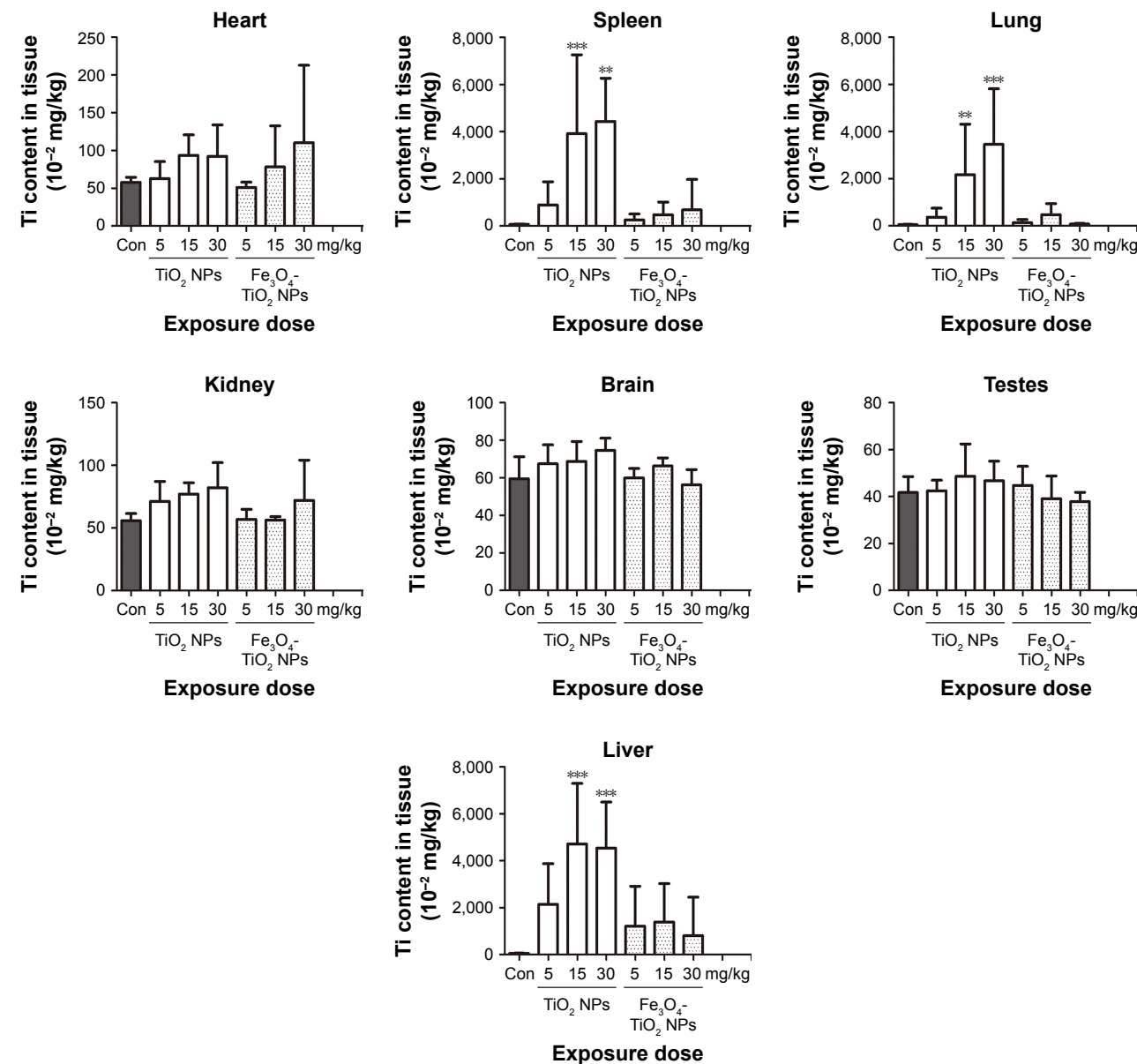


Figure 3 Ti content in tissue of rats after treatment with Fe₃O₄-TiO₂ NPs and TiO₂ NPs.

Note: **P<0.01, ***P<0.001 compared with control.

Abbreviations: NPs, nanoparticles; Con, control.

risk of infection. This result was in agreement with the lymphoid aggregates found in liver tissue at the 5 mg/kg TiO₂ NPs dose.

In this study, no obvious pathological changes were observed in the histology of the heart in any treatment group. A significant decrease in CK levels was found only in 5 mg/kg TiO₂ NP-treated animals. However, a significant decrease in CK-MB levels was found in all Fe₃O₄-TiO₂ NP-treated animals and 30 mg/kg TiO₂ NP-treated animals. Normally, CK-MB is produced mainly by the myocardium and liver. Muscles can also produce a small amount of

CK-MB.²⁶ The cause of the decrease in CK-MB levels is not clear, and more studies are necessary in order to clarify the exact mechanism of this phenomenon.

Previous research has shown that TiO₂ NP treatment through oral administration can increase hepatocyte necrosis.²⁷ Our study showed that TiO₂ NPs accumulated in the liver, spleen, and lungs, which suggests that these organs might be the major places where TiO₂ NPs were metabolized. Fabian et al investigated tissue distribution after intravenous administration of TiO₂ NPs and found that the levels were highest in the liver, followed by the spleen and lungs.²⁸

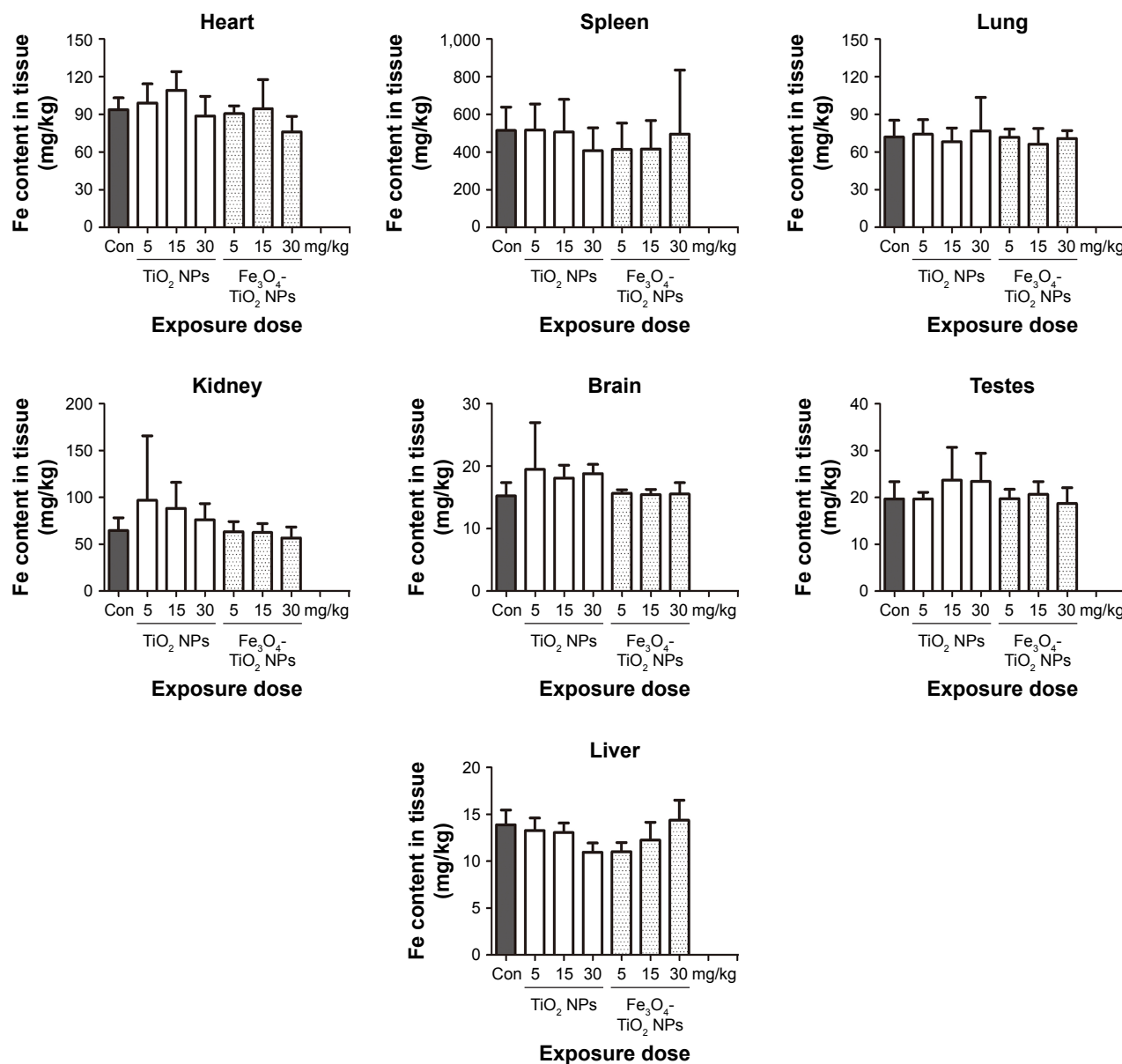


Figure 4 Fe content in tissue of rats after treatment with $\text{Fe}_3\text{O}_4\text{-TiO}_2$ NPs or TiO_2 NPs.
Abbreviations: NPs, nanoparticles; Con, control.

Mohamed and Hussien also confirmed that when TiO_2 NPs enter the blood, it is very easy for the particles to reach and accumulate in the most critical organs of the body, such as the brain, spleen, liver, kidneys, and lungs, causing injury to these organs and tissue.²⁹ Many studies have shown that accumulation of TiO_2 NPs can be observed in the liver, lungs, kidneys, and spleen after intravenous, intraperitoneal, or dermal administration.^{22,28,30}

Interestingly, in this study, we found no significant increase in Ti content in the liver, spleen, or lungs in any of the $\text{Fe}_3\text{O}_4\text{-TiO}_2$ NP-treatment groups when compared with

controls. ICP-MS analysis showed a very small amount of Ti accumulation in the kidneys and spleen in $\text{Fe}_3\text{O}_4\text{-TiO}_2$ NP-treatment groups, but there was no significant accumulation in brain tissue. The results may partly explain why Ti accumulation, histopathological changes, hepatocyte apoptosis of the liver, and a certain degree of alteration in liver function was more severe in the TiO_2 NP-treatment groups than the $\text{Fe}_3\text{O}_4\text{-TiO}_2$ NP groups. The reason for this phenomenon might be the interaction of Fe_3O_4 with TiO_2 NPs. Fe_3O_4 seems to act as a beneficial factor in Janus $\text{Fe}_3\text{O}_4\text{-TiO}_2$ NP-metabolism process in the body.

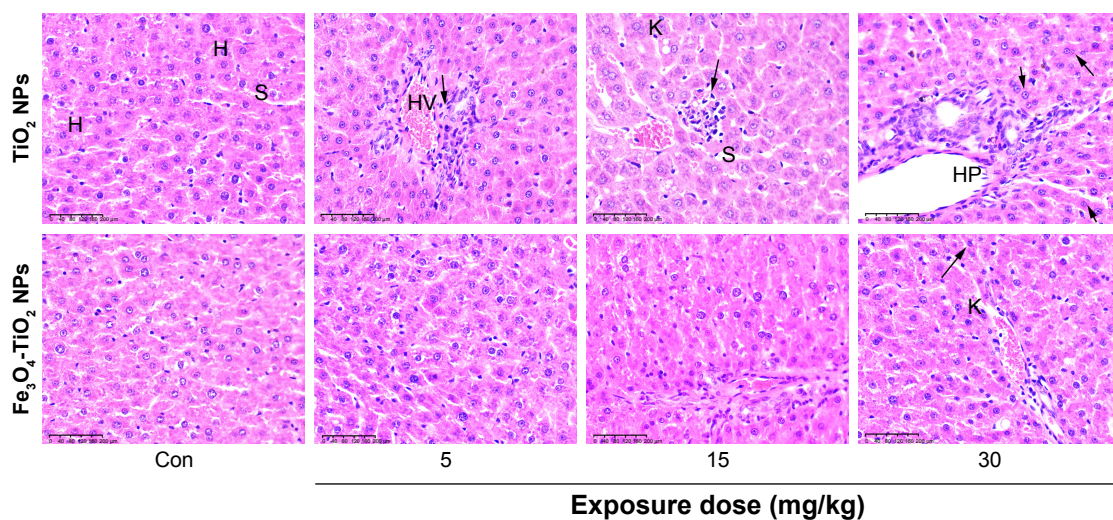


Figure 5 Photomicrography of liver histopathology.

Notes: Images (magnification 10 \times) represent histopathological sections of the liver. Arrows represent small focal-like inflammatory cell infiltration around the hepatic portal (HP) area in the 5 mg/kg TiO_2 NP group and around the hepatic vein (HV) in the 15 mg/kg TiO_2 NP group, and lymphocyte aggregation in the 30 mg/kg TiO_2 NP group. Dark arrows represent liver hepatocyte (H) granule degeneration and small stove liver-cell shrinkage in both Fe_3O_4 - TiO_2 NP and TiO_2 NP groups at 30 mg/kg.

Abbreviations: NPs, nanoparticles; Con, control; S, sinus; K, Kupffer cells.

Although TiO_2 has been classified by the International Agency for Research on Cancer as a group 2B carcinogen, human epidemiological studies on TiO_2 have provided inadequate evidence of carcinogenicity. Research indicates that delayed hypersensitivity to Ti and its oxides may induce a health risk for individuals with higher susceptibility.³¹ Therefore, excessive Ti accumulation in the body over a long period has the potential to induce certain adverse effects in the body.

To check how the molecular mechanism of TiO_2 NP and Fe_3O_4 - TiO_2 NP treatment affected the rat liver, the signaling cascade of stress-activated MAPK-pathway-related proteins were detected. Recent studies in vivo have shown that the MAPK cascade converging on JNK and p38 plays a central role.³² Among the three MAPKs, ERK is activated by various cytokines and growth factors and plays a central role in cell growth and differentiation.³³ Research has shown that JNK can mediate both cell-survival and cell-death pathways,

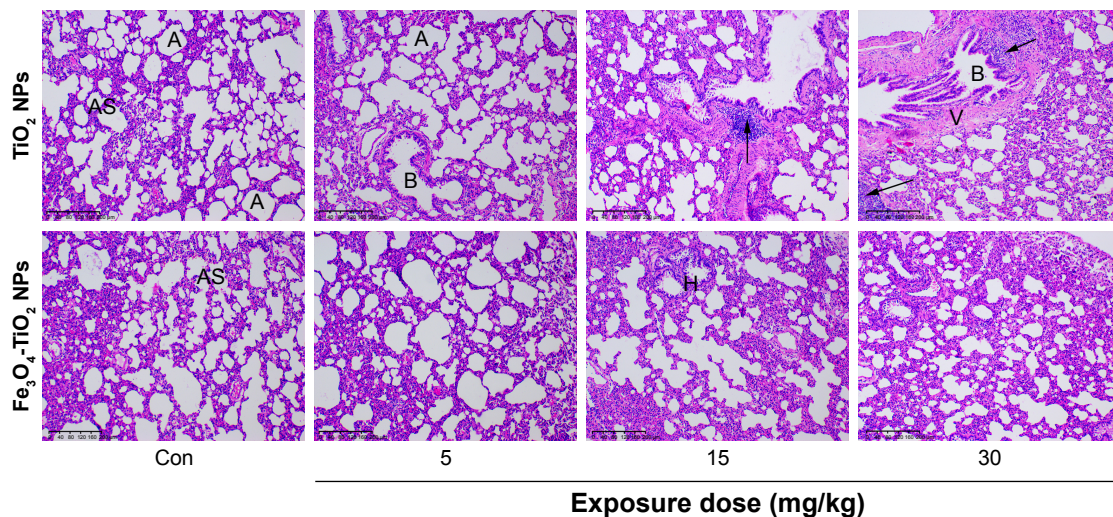


Figure 6 Photomicrography of lung histopathology.

Notes: Images (magnification 10 \times) represent histopathological sections of the lung. Dark arrow in the 15 mg/kg TiO_2 NP group represents edema and exudation around bronchi and a large amount of inflammatory cell infiltration. Dark arrows in the 30 mg/kg TiO_2 NP group represent a large number of inflammatory infiltration around bronchi.

Abbreviations: NP, nanoparticle; Con, control; A, alveolar space; B, bronchioles; H, histiocytes; AS, alveolar septa; V, veins.

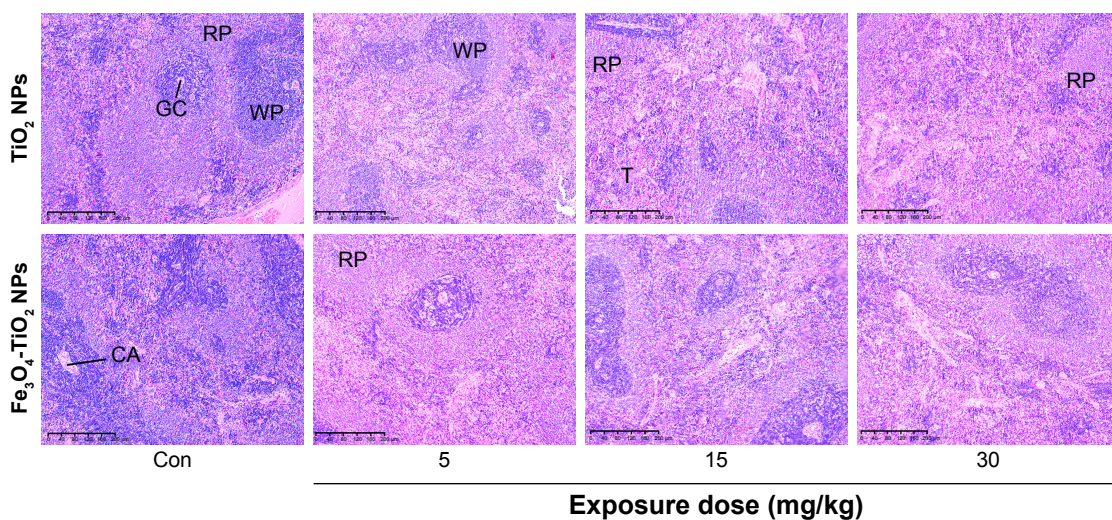


Figure 7 Photomicrography of spleen histopathology.

Note: Images (magnification 10 \times) represent histopathological sections of the spleen.

Abbreviations: NPs, nanoparticles; Con, control; RP, red pulp; WP, white pulp; T, trabeculae; CA, central artery; GC, germinal center.

which are often determined by the duration of JNK activation. Sustained JNK is important in mediating apoptosis and necrosis.^{34,35} JNK signaling is associated with survival, cell death, differentiation, proliferation, and tumorigenesis in hepatocytes. In nonparenchymal liver cells, such as hepatic macrophages (Kupffer cells) and hepatic stellate cells, JNK is involved in inflammation and fibrosis.³⁶ JNK and p38 MAPKs, also called stress-activated MAPKs, are preferentially activated by proinflammatory cytokines, such as TNF α , and environmental and genotoxic stresses. After activation, stress-activated MAPKs phosphorylate specific

serine/threonine residues of target substrates and exert a variety of cellular functions, such as cell death, survival, proliferation, migration, and inflammation.

In this study, Western blot analysis revealed that ERK increased in the 30 mg/kg $\text{Fe}_3\text{O}_4\text{-TiO}_2$ NP group. A significant increase in expression of JNK and p-JNK in liver tissue occurred in both $\text{Fe}_3\text{O}_4\text{-TiO}_2$ NP- and TiO_2 NP-treatment groups compared to controls. Expression of p-p38 was increased in the 5 mg/kg TiO_2 NP group. These results suggest that both $\text{Fe}_3\text{O}_4\text{-TiO}_2$ NPs and TiO_2 NPs have certain effects on MAPK-cascade proteins.

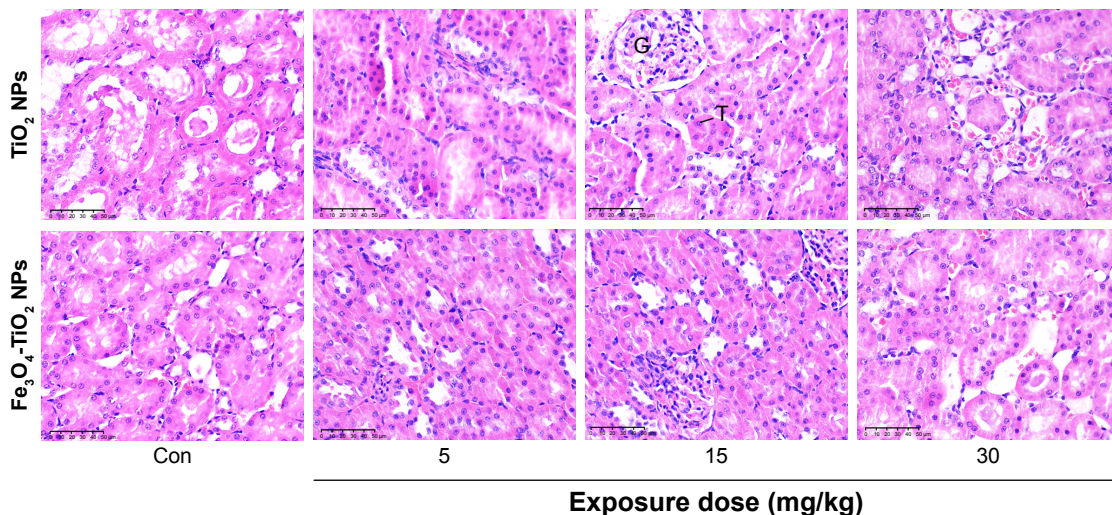


Figure 8 Photomicrography of kidney histopathology.

Notes: Images (magnification 40 \times) represent histopathological sections of kidneys. No significant pathological changes were observed in the hearts in either $\text{Fe}_3\text{O}_4\text{-TiO}_2$ NPs or TiO_2 NPs treated animals (data not shown).

Abbreviations: NPs, nanoparticles; Con, control; G, glomerular; T, tubular epithelial cells.

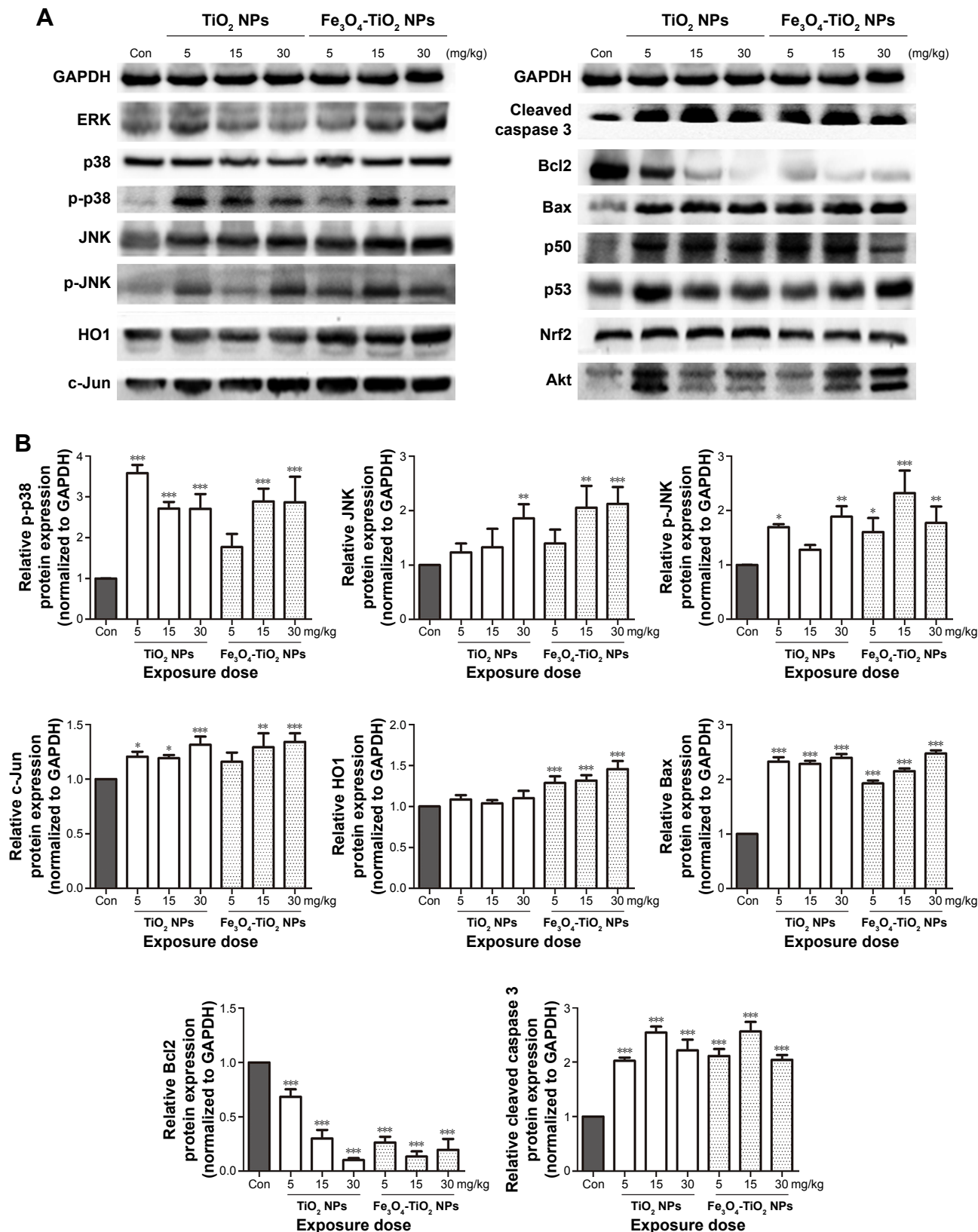


Figure 9 Signal protein expression in liver tissue.

Notes: (A) Protein-expression levels of p38, p-p38, JNK, p-JNK, HO1, ERK, c-Jun, cleaved caspase 3, Bcl2, Bax, p50, p53, Nrf2, Akt, and GAPDH; (B) relative protein expression (normalized to GAPDH). * $P<0.05$, ** $P<0.01$, *** $P<0.001$ compared with control.

Abbreviations: NPs, nanoparticles; Con, control.

Signal pathways involved in apoptosis were also investigated in this study. We found that both $\text{Fe}_3\text{O}_4\text{-TiO}_2$ NPs and TiO_2 NPs significantly increased expression of the proapoptotic proteins Bax and cleaved caspase 3, but decreased expression of the antiapoptotic protein Bcl2. Bcl2 inhibits apoptosis, while Bax promotes apoptosis, and the ratio of the Bcl2–Bax protein complex is directly related to the occurrence of apoptosis. Some researchers have even named the Bcl2:Bax ratio the “apoptosis switch”. When the Bax protein is dominant, apoptosis occurs, whereas when the Bcl2 protein is dominant, the cell survives.³⁷ The reason the intensity of Bcl2- and Bax-expression bands obtained in this study seems not to follow a correlated pattern might be the difference in incubation and development times of different membranes during our Western blot experiments. Cleaved caspase 3 expression means activation of cell-death protease. HO1 expression increased in all treatment groups, especially $\text{Fe}_3\text{O}_4\text{-TiO}_2$ NP groups. Under normal physiological conditions, the expression and vitality of HO1 are low. As a stress-responsive protein, HO1 can be activated under different stress conditions and has a strong antioxidant effect.³⁸ Nrf2 is a transcription factor and has been shown to play an essential role in the antioxidant response element-mediated expression of phase 2 detoxifying enzymes and stress-inducible genes.³⁹ Nrf2-protein expression in liver tissue showed no significant change in any of the treated groups. Our results suggest that both $\text{Fe}_3\text{O}_4\text{-TiO}_2$ NPs and TiO_2 NPs activated oxidative- and antioxidative-related signal proteins in rat liver cells, although certain differences may exist between the two materials.

Intravenous injection of $\text{Fe}_3\text{O}_4\text{-TiO}_2$ NPs led to slight inflammation in lungs, kidneys, and spleen

Renal profiles showed that UrcA in all $\text{Fe}_3\text{O}_4\text{-TiO}_2$ NP-treatment groups were significantly decreased in a dose-response manner. Low UrcA may occur by numerous causes, such as low dietary zinc intake. Wang et al suggested that serum-UrcA levels lower than healthy controls could be used as a useful biomarker for multiple sclerosis diagnosis.⁴⁰ Serum LDL-C levels with TiO_2 NP treatment at 5 mg/kg and $\text{Fe}_3\text{O}_4\text{-TiO}_2$ NP treatment at 30 mg/kg were significantly higher than controls. High LDL-C levels in the blood may deposit in the heart, brain, or other parts of the artery wall, and gradually form atherosclerotic plaques, blocking the corresponding blood vessels. An increase in serum LDL-C levels is often used to evaluate the risk of future heart disease.⁴¹

In the spleen and lungs, Ti content increased significantly in the 15 and 30 mg/kg TiO_2 NP-treatment groups compared to controls. However, no significant increases in Ti content in the spleen or lungs in any of the $\text{Fe}_3\text{O}_4\text{-TiO}_2$ NP-treatment groups was observed. These results indicate that compared to $\text{Fe}_3\text{O}_4\text{-TiO}_2$ NPs, TiO_2 NPs seem to be accumulated more easily in the lung and spleen, which then brings harmful risks to the organs.

Lung histopathological examination showed that mild and focal inflammatory infiltrates in the pulmonary parenchyma in both $\text{Fe}_3\text{O}_4\text{-TiO}_2$ NP- and TiO_2 NP-treated rats, suggesting that slight inflammation occurred. An increase in red-pulp area can be caused by different pathological conditions, such as portal hypertension, cardiac failure, or extramedullary hematopoiesis. Spleen histopathological examination indicated that in the TiO_2 NP-treatment group at 15 mg/kg, the red-pulp area in the spleen increased when compared with the same dose in the $\text{Fe}_3\text{O}_4\text{-TiO}_2$ NP group.

The electrolyte profile showed a significant decrease in potassium in the 15 mg/kg $\text{Fe}_3\text{O}_4\text{-TiO}_2$ NP group, while other groups also showed a decrease, but without any statistical difference. Martínez-Valles et al found that hypokalemia was associated with small-cell lung cancer.⁴² Serum phosphate was significantly decreased at 5 and 30 mg/kg in the $\text{Fe}_3\text{O}_4\text{-TiO}_2$ NP groups, and TiO_2 NPs at 15 mg/kg also showed a significant decrease. Organic phosphorus is essential for numerous normal physiological functions, including skeletal development, mineral metabolism, cell-membrane phospholipid content and function, energy transfer through mitochondrial metabolism, and cell signaling. Although serum phosphate reflects only a minor fraction of total body phosphorus, this decrease may cause a reduction in urinary phosphorus excretion, which may further lead to metabolic acidosis and a decrease in growth and thyroid hormones.⁴³ Serum chlorine in the $\text{Fe}_3\text{O}_4\text{-TiO}_2$ NP treatment at 30 mg/kg group showed a significant increase. An increase in serum-chlorine levels has been linked to renal disease, renal failure, and renal tubular acidosis.⁴⁴ No obvious pathological changes were observed in the brain, heart, or testes in any of the treatment groups in this study. Due to the uncertainty in the extrapolation of toxicological data from experimental animals to humans, more studies will be needed before elaborating on detailed mechanisms of these findings and the biosafety of $\text{Fe}_3\text{O}_4\text{-TiO}_2$ NPs for clinical use.⁴⁵

Conclusion

In summary, the major findings of the present study include a certain degree of alteration in liver function and electrolyte

and lipid parameters in both Fe_3O_4 - TiO_2 NP- and TiO_2 NP-treated rats. Both materials induced a certain degree of damage in lungs, spleen, liver, and kidneys. To a certain degree, we conclude that Janus Fe_3O_4 - TiO_2 NPs are less toxic than TiO_2 NPs in animal experiments. The data from this study provide pharmacokinetic and biokinetic information for Janus Fe_3O_4 - TiO_2 NPs. This will be very important in determining the biosafety of Fe_3O_4 - TiO_2 NP use in nanomedicine.

Acknowledgments

The authors would like to thank Ms Linda Bowman for her assistance in the preparation of this article. This work was partly supported by the National Nature Science Foundation of China (grant 81273111), Scientific Projects of Zhejiang Province (2015C33148 and 2015C37117), the Scientific Innovation Team for Environmental Hazardous Factor Control and Prevention (2016C51001), Zhejiang Key Laboratory of Pathophysiology (201703), and the KC Wong Magna Fund in Ningbo University.

Disclosure

The authors report no conflicts of interest in this work.

References

1. Su H, Wang Y, Gu Y, Bowman L, Zhao J, Ding M. Potential applications and human biosafety of nanomaterials used in nanomedicine. *J Appl Toxicol*. 2018;38(1):3–24.
2. Zhang M, Zhang L, Chen Y, Li L, Su Z, Wang C. Precise synthesis of unique polydopamine/mesoporous calcium phosphate hollow Janus nanoparticles for imaging-guided chemo-photothermal synergistic therapy. *Chem Sci*. 2017;8(12):8067–8077.
3. Wang Y, Ding T, Baumberg JJ, Smoukov SK. Symmetry breaking polymerization: one-pot synthesis of plasmonic hybrid Janus nanoparticles. *Nanoscale*. 2015;7(23):10344–10349.
4. Yi Y, Sanchez L, Gao Y, Yu Y. Janus particles for biological imaging and sensing. *Analyst*. 2016;141(12):3526–3539.
5. Tran LT, Lesieur S, Faivre V. Janus nanoparticles: materials, preparation and recent advances in drug delivery. *Expert Opin Drug Deliv*. 2014;11(7):1061–1074.
6. Chen X, Li G, Han Q, et al. Rational Design of Branched Au- Fe_3O_4 Janus Nanoparticles for Simultaneous Trimodal Imaging and Photothermal Therapy of Cancer Cells. *Chemistry*. 2017;23(68):17204–17208.
7. Shin TH, Choi Y, Kim S, Cheon J. Recent advances in magnetic nanoparticle-based multi-modal imaging. *Chem Soc Rev*. 2015;44(14):4501–4516.
8. Miyoshi N, Kume K, Tsutumi K. Application of Titanium Dioxide (TiO_2)Nanoparticles in Photodynamic Therapy (PDT) of an Experimental Tumor. *AIP Conference Proceedings*. 2011;1415(1):21–23.
9. Hasanzadeh H. Stabilizing and dispersing methods of TiO_2 nanoparticles in biological studies. *J Paramed Sci*. 2015;6(2):96–105.
10. Deng CY, Long YY, Liu S, Chen ZB, Li C. Construction of biotin-modified polymeric micelles for pancreatic cancer targeted photodynamic therapy. *Yao Xue Xue Bao*. 2015;50(8):1038–1044.
11. Rosen JE, Yoffe S, Meerasa A. Nanotechnology and Diagnostic Imaging: New Advances in Contrast Agent Technology. *J Nanomed Nanotechnol*. 2011;02(05):5.
12. Junsung P, Wonkyung C, Jun PH. Biodistribution of newly synthesized PHEA-based polymer-coated SPION in Sprague Dawley rats as magnetic resonance contrast agent. *Int J Nanomedicine*. 2014;2014 (Issue 1):4077–4089.
13. Vogl TJ, Hammerstingl R, Schwarz W, et al. Magnetic resonance imaging of focal liver lesions. Comparison of the superparamagnetic iron oxide resovist versus gadolinium-DTPA in the same patient. *Invest Radiol*. 1996;31(11):696–708.
14. Zeng L, Ren W, Xiang L, Zheng J, Chen B, Wu A. Multifunctional Fe_3O_4 - TiO_2 nanocomposites for magnetic resonance imaging and potential photodynamic therapy. *Nanoscale*. 2013;5(5):2107–2113.
15. Li Q, Wang X, Lu X, et al. The incorporation of daunorubicin in cancer cells through the use of titanium dioxide whiskers. *Biomaterials*. 2009;30(27):4708–4715.
16. Wang Y, Cui H, Zhou J, et al. Cytotoxicity, DNA damage, and apoptosis induced by titanium dioxide nanoparticles in human non-small cell lung cancer A549 cells. *Environ Sci Pollut Res Int*. 2015;22(7):5519–5530.
17. Shukla RK, Kumar A, Vallabani NV, Pandey AK, Dhawan A. Titanium dioxide nanoparticle-induced oxidative stress triggers DNA damage and hepatic injury in mice. *Nanomedicine (Lond)*. 2014;9(9):1423–1434.
18. Xie Y, Liu D, Cai C, et al. Size-dependent cytotoxicity of Fe_3O_4 nanoparticles induced by biphasic regulation of oxidative stress in different human hepatoma cells. *Int J Nanomedicine*. 2016;11:3557–3570.
19. Liu G, Gao J, Ai H, Chen X. Applications and potential toxicity of magnetic iron oxide nanoparticles. *Small*. 2013;9(9–10):1533–1545.
20. Zhao J, Castranova V. Toxicology of Nanomaterials Used in Nanomedicine. *J Toxicol Environ Health B Crit Rev*. 2011;14(8):593–632.
21. Dinh CT, Nguyen TD, Kleitz F, Do TO. Shape-controlled synthesis of highly crystalline titania nanocrystals. *ACS Nano*. 2009;3(11):3737–3743.
22. Krystek P, Tentschert J, Nia Y, et al. Method development and inter-laboratory comparison about the determination of titanium from titanium dioxide nanoparticles in tissues by inductively coupled plasma mass spectrometry. *Anal Bioanal Chem*. 2014;406(16):3853–3861.
23. Zhang XD, Wu HY, Wu D, et al. Toxicologic effects of gold nanoparticles in vivo by different administration routes. *Int J Nanomedicine*. 2010;5(1):771–781.
24. Janz TG, Hamilton GC. Anemia, Polycythemia, and White Blood Cell Disorders. In: Marx J, Hockberger R, Walls R, Adams J, Rosen P, editors. *Rosen's Emergency Medicine – Concepts and Clinical Practice*. 7th edition. Philadelphia: Mosby/Elsevier; 2010:1586–1605.
25. Aster JC. Diseases of white blood cells, lymph nodes, spleen and thymus. Robbins and Cotran Pathologic Basis of Disease; 2005:661–709.
26. Shao J. Effect of aqueous extract of *Lycium barbarum* on serum CK, CK-MB activities and myocardium injury in exhausted swimming rats. *J Med Plant Res*. 2011;5(14):3335–3337.
27. Wang J, Zhou G, Chen C, et al. Acute toxicity and biodistribution of different sized titanium dioxide particles in mice after oral administration. *Toxicol Lett*. 2007;168(2):176–185.
28. Fabian E, Landsiedel R, Ma-Hock L, Wiench K, Wohlleben W, van Ravenzwaay B. Tissue distribution and toxicity of intravenously administered titanium dioxide nanoparticles in rats. *Arch Toxicol*. 2008;82(3):151–157.
29. Mohamed HRH, Hussien NA. Genotoxicity Studies of Titanium Dioxide Nanoparticles (TiO_2 NPs) in the Brain of Mice. *Scientifica (Cairo)*. 2016;2016:6710840.
30. Chen J, Dong X, Zhao J, Tang G. In vivo acute toxicity of titanium dioxide nanoparticles to mice after intraperitoneal injection. *J Appl Toxicol*. 2009;29(4):330–337.
31. Skocaj M, Filipic M, Petkovic J, Novak S. Titanium dioxide in our everyday life; is it safe? *Radiol Oncol*. 2011;45(4):227–247.
32. Nakagawa H, Maeda S. Molecular mechanisms of liver injury and hepatocarcinogenesis: focusing on the role of stress-activated MAPK. *Patholog Res Int*. 2012;2012:172894.
33. Munshi A, Ramesh R. Mitogen-activated protein kinases and their role in radiation response. *Genes Cancer*. 2013;4(9–10):401–408.

34. Win S, Than TA, Han D, Petrovic LM, Kaplowitz N. c-Jun N-terminal kinase (JNK)-dependent acute liver injury from acetaminophen or tumor necrosis factor (TNF) requires mitochondrial Sab protein expression in mice. *J Biol Chem*. 2011;286(40):35071–35078.
35. Johnson GL, Nakamura K. The c-jun kinase/stress-activated pathway: regulation, function and role in human disease. *Biochim Biophys Acta*. 2007;1773(8):1341–1348.
36. Seki E, Brenner DA, Karin M. A liver full of JNK: signaling in regulation of cell function and disease pathogenesis, and clinical approaches. *Gastroenterology*. 2012;143(2):307–320.
37. Ramalho RM, Cortez-Pinto H, Castro RE, et al. Apoptosis and Bcl-2 expression in the livers of patients with steatohepatitis. *Eur J Gastroenterol Hepatol*. 2006;18(1):21–29.
38. Nguyen T, Yang CS, Pickett CB. The pathways and molecular mechanisms regulating Nrf2 activation in response to chemical stress. *Free Radic Biol Med*. 2004;37(4):433–441.
39. Wei CC, Kong YY, Li GQ, Guan YF, Wang P, Miao CY. Nicotinamide mononucleotide attenuates brain injury after intracerebral hemorrhage by activating Nrf2/HO-1 signaling pathway. *Sci Rep*. 2017;7(1):717.
40. Wang L, Hu W, Wang J, Qian W, Xiao H. Low serum uric acid levels in patients with multiple sclerosis and neuromyelitis optica: An updated meta-analysis. *Mult Scler Relat Disord*. 2016;9:17–22.
41. Dickerson JB, McNeal CJ, Tsai G, et al. Can an Internet-based health risk assessment highlight problems of heart disease risk factor awareness? A cross-sectional analysis. *J Med Internet Res*. 2014;16(4):e106.
42. Martínez-Valles MA, Palafox-Cazarez A, Paredes-Avina JA. Severe hypokalemia, metabolic alkalosis and hypertension in a 54 year old male with ectopic ACTH syndrome: a case report. *Cases J*. 2009;2(1):6174.
43. Moe SM. Disorders involving calcium, phosphorus, and magnesium. *Primary Care Clinics in Office Practice*. 2008;35(2):215–237.
44. Nagami GT. Hipercloremia: por qué y cómo [Hyperchloraemia: why and how]. *Nefrología*. 2016;36(4):347–353. Spanish.
45. Gordon CJ. Toxic-induced hypothermia and hypometabolism: do they increase uncertainty in the extrapolation of toxicological data from experimental animals to humans? *Neurosci Biobehav Rev*. 1991; 15(1):95–98.

International Journal of Nanomedicine

Publish your work in this journal

The International Journal of Nanomedicine is an international, peer-reviewed journal focusing on the application of nanotechnology in diagnostics, therapeutics, and drug delivery systems throughout the biomedical field. This journal is indexed on PubMed Central, MedLine, CAS, SciSearch®, Current Contents®/Clinical Medicine,

Submit your manuscript here: <http://www.dovepress.com/international-journal-of-nanomedicine-journal>

Dovepress

Journal Citation Reports/Science Edition, EMBase, Scopus and the Elsevier Bibliographic databases. The manuscript management system is completely online and includes a very quick and fair peer-review system, which is all easy to use. Visit <http://www.dovepress.com/testimonials.php> to read real quotes from published authors.